nature physics

ARTICLES

https://doi.org/10.1038/s41567-018-0389-0

# Direct observation of ion acceleration from a beam-driven wave in a magnetic fusion experiment

R. M. Magee *, A. Necas, R. Clary, S. Korepanov, S. Nicks, T. Roche, M. C. Thompson, M. W. Binderbauer and T. Tajima

**Efficiently heating a magnetically confined plasma to thermonuclear temperatures remains a central issue in fusion energy research. One well-established technique is to inject beams of neutral particles into the plasma, a process known as neutral beam injection. In the classical picture, fast ions generated from neutral beam injection predominantly heat electrons as they are slowed by friction. This electron heat is then collisionally coupled to the plasma ions, which comprise the fusion fuel. Fast ions can also drive plasma waves, which divert energy from the fuel and can degrade confinement. Here we present new observations from a field reversed configuration plasma in which a beam-driven wave in the open field line region couples directly to fuel ions, drawing a high-energy tail on subcollisional timescales that dramatically enhances the fusion rate. This mode therefore allows the beam energy to bypass the electron channel and does so without having a deleterious effect on global plasma confinement. Our results demonstrate a means of directly and non-destructively coupling energy from fast ions to plasma ions, which may pave the way for improved neutral beam injection heating efficiency or the prevention of ash accumulation with alpha channelling.**

The C-2U advanced, beam-driven field reversed configuration (FRC)[1] experiment is composed of a high-density, prolate toroid with low internal magnetic field embedded in the linear open field line plasma of a magnetic mirror. Tangential neutral beam injection (NBI) creates a population of fast ions whose orbits encircle the toroid, dipping in and out of the closed flux surface region as they execute betatron-like orbits (Fig. 1). These features of low field and tangential injection create a fast ion environment that is unique among magnetic fusion energy devices. In the tokamak, for example, the ratio of the fast ion orbit radius to the plasma radius is typically a few percent. Here, it is ~1. This large fast ion orbit size allows the particles to average over small scale fluctuations[2], resulting in a fast ion lifetime near the classical limit[3].

A further distinguishing feature of C-2U is the high NBI power density. The ratio of the injected beam power to plasma volume is roughly an order of magnitude larger than in the Joint European Torus, the most powerful tokamak in the world. High NBI power density coupled with good fast ion confinement results in the rapid accumulation of fast ions in the plasma. In fact, by about 1 ms into the discharge (the time for a test ion to slow by $1/e$), the fast ion pressure becomes approximately equal to the plasma thermal pressure.

This dominant fast ion population affects the global plasma in several ways. It stabilizes the plasma[3,4], sustains the plasma against resistive decay[5,6], and suppresses low-frequency turbulence[7,8]. Each of these has been described elsewhere. The focus of the present work is a remarkable, newly observed mode of ion energization. While beam-driven waves are common in magnetic fusion energy[9], they usually degrade the confinement properties of the plasma[10] or clamp the achievable fast ion density[11]. In our case, there is no observed confinement degradation or fast ion density limit with the appearance of the mode. Instead, we observe the creation of a large population of 'tail' ions: ions from the thermal populations that are accelerated to many times the thermal energy on subcollisional timescales. This is, to our knowledge, the first observation of plasma ions gaining energy from beam-driven waves in a magnetic fusion device (although theoretical mechanisms have been proposed[12]).

## Background

The Alfvén velocity is a fundamental plasma property, given by $V_A = B/\sqrt{\mu_0 \rho}$ where $B$ is the magnetic field strength, $\mu_0$ is the permeability of free space and $\rho$ is the mass density of the plasma. Beam particles injected into a plasma with velocity $v_b > V_A$ can, like a speedboat through water, drive waves. The free energy source for the waves can be positive velocity space gradients (that is, $\partial f/\partial v > 0$, where $f$ is the ion velocity distribution function) or spatial gradients[13]. If the phase velocity of these waves, $v_\phi$, is much larger than the plasma ion thermal velocity, $v_{T,i}$ (and much smaller than the electron thermal velocity), the wave is not immediately damped and can grow to large amplitude. These large-amplitude waves can then resonate with plasma particles through one of a variety of mechanisms, and significant tail energization will occur. As we discuss below, these three conditions—(1) $v_b > V_A$, (2) $\partial f/\partial v > 0$ and (3) $v_\phi \gg v_{T,i}$)—are precisely met in the open field line region of the C-2U plasma (yellow tubes in Fig. 1), and so it is there where we expect to find the most virulent beam-driven mode activity.

In this Article we present a collection of experimental observations related to the newly discovered phenomenon, including magnetic field and density fluctuations, suprathermal neutron production and direct measurements of a high energy tail of plasma ions. An electromagnetic particle-in-cell (PIC) simulation in a simplified geometry is used to identify the mode, and connections are made to both the experimental observations and analytic theory. Finally, a dedicated experiment is conducted that illustrates how the mode can be controlled by manipulation of the free energy source, the neutral beam velocity distribution.

## Observations

One product of the deuterium–deuterium fusion reaction comprises 2.45 MeV neutrons. The fusion rate of the plasma depends

TAE Technologies, Inc., Foothill Ranch, CA, USA. *e-mail: RMagee@TAE.com

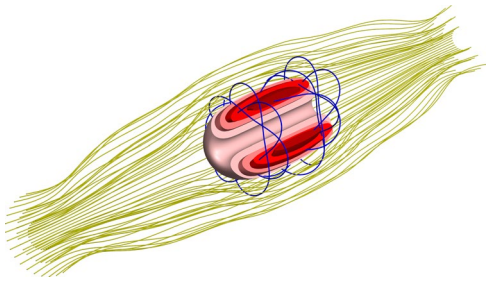

**Fig. 1 | Illustration of the FRC.** The FRC is shown as a solid body (with cut-away) with closed field line surfaces (red shells) embedded in the mirror plasma (yellow tubes). A sample 7 keV fast ion trajectory is shown in blue.

on the densities and temperatures of the reactants and the reaction cross-section. Two absolutely calibrated[14] scintillator-based neutron detectors are located close to the vessel wall on the atmosphere side. The FRC plasma is pure deuterium and the neutral beams are pure hydrogen. There is therefore no beam-plasma component to the neutron production, and neutrons are produced only due to fusion reactions between plasma ions themselves. That the beams are deuterium-free is confirmed experimentally by firing the beams into the deuterated vessel wall and measuring zero neutron signal.

Shown in Fig. 2c is the shot-averaged measured rate (black line with salmon error bars) and the calculated thermonuclear rate (purple diamonds). It can be seen that the measured rate exceeds the thermonuclear rate from very early on in the discharge. The thermonuclear rate is calculated as $R=\frac{1}{2}2\pi L_{\mathrm{FRC}}\int n_{\mathrm{i}}(r)^2<\sigma v>(T_{\mathrm{i}}(r))r\,\mathrm{d}r$ where $L_{\mathrm{FRC}}$ is the length of the FRC obtained from magnetic measurements of excluded flux[15], $n_{\mathrm{i}}(r)$ is the ion density, which we obtain from Abel-inverted interferometry measurements[16] of $n_{\mathrm{e}}(r)$ and assuming quasi-neutrality ($n_{\mathrm{i}}\sim n_{\mathrm{e}}$). The ion temperature, $T_{\mathrm{i}}(r)$, is calculated using radial pressure balance to determine the total internal pressure and subtracting the contribution for electrons, whose temperature is measured with Thomson scattering (see Methods for details).

The measured neutron rate clearly diverges from the calculated rate very early in time. This timescale is much faster than the timescale for collisional heating of plasma ions by beam particles. A fast test particle with velocity between the ion and electron thermal velocity must slow to the critical energy before it will have a significant probability of pitch angle scattering on plasma ions (the critical energy is the energy at which power flow to the ions and electrons is equal)[17]. In our case, the injected ions have, $E_{\mathrm{fi}}=10E_{\mathrm{crit}}$ and therefore two to three e-folding times (2–4 ms) must pass before significant energy flow to the ions is expected.

In addition to measurements of the neutron flux, we measured the intermittent magnetic and density fluctuations near the plasma ion cyclotron frequency. The magnetic fluctuations were measured ~10 cm inside the wall in the mirror plasma with a high-time-resolution magnetic probe and the density fluctuations with far infrared (FIR) interferometry[18] from four different viewing chords (impact parameters $r=0$, 15, 30, 45 cm). The magnetic probe measurements revealed mode activity at the fundamental and higher harmonics of the ion cyclotron frequency (Fig. 3c). The density fluctuations reveal that there is an electrostatic component to the mode and that it is not confined to the FRC, as the fluctuations appear on the $r=45$ cm chord, which does not intersect the FRC. In fact, the relative size of the line-integrated fluctuations (that is, $\delta\int n\mathrm{d}l/\int n\mathrm{d}l$) is largest on this most-outboard chord, outside the separatrix.

To investigate the source of the fusion enhancement, we used a high-resolution, $E||B$ neutral particle energy analyser (NPA) with 39 energy channels per species to directly measure the evolution of both the bulk deuterium and injected hydrogen energy spectra[19]. The line of sight of the NPA has a large impact parameter ($b=49$ cm) so it does not measure ions in the FRC core, and with a minimum energy of 1 keV, the detector is not sensitive to the thermal population. An average of seven similar shots is shown in Fig. 4. Early in time ($t<1$ ms), there is a large energetic deuterium population due to FRC formation (the FRC is formed by the collision and merger of two supersonic compact toroids[4]). The NBI fast hydrogen population is born at 15 keV, but rapidly fills in as the fast ions slow down and accumulate in the plasma. At about $t=1$ ms, a broad tail appears in the deuterium channels, centred at 12 keV. The tail persists for several milliseconds until the FRC begins to decay away. The deuterium ions do not show the characteristic slowing down that the injected hydrogen ions do because at this large radius the more massive deuterium ions are not confined. It is also important to note that the amplitude of the NPA signal from the tail is comparable to that of the signal from the injected beam ions, so nuclear elastic scattering or 'knock-on'[20] can be excluded as a candidate mechanism.

The temporal behaviour of the measured neutron rate trends very well with the temporal behaviour of the rate calculated using the energy spectrum measured by the NPA. This stands in stark contrast to Fig. 2, where the temporal behaviours of the calculated and measured rates differ as greatly as the amplitudes. The rate is calculated here assuming the fusion collisions are dominantly between energetic tail ions and bulk plasma ions as $R\sim\int \mathrm{d}Ef(E)\sigma_{\mathrm{DD}}(E)v$ where $f(E)$ is the NPA energy spectrum, $\sigma_{\mathrm{DD}}$ is the fusion cross-section, and $v$ is the ion velocity (plasma temperature is ignored here). Although the tail is measured to exist in the tenuous mirror plasma, the low magnetic field means that the fast ions have large orbits and can travel into the FRC where the larger plasma ion density makes fusion more likely. The result is over-plotted on the measurement in Fig. 4c. The excellent agreement between the two curves is compelling evidence that the neutron production is dominated by the high-energy tail interacting with the thermal plasma, rather than from within the thermal population itself.

It should be noted that the number of suprathermal ions is small, ~1% of the background ion population based on the neutron flux. The energy per particle, however, is large (~12 keV), so the total energy is therefore not insignificant. At ~500 J, the energy in the tail is approximately 10% of the total thermal energy of the plasma. The characteristic time for the tail to grow up is ~1 ms, a time during which 10 kJ of neutral beam power can accumulate in the plasma. This means ~5% of the injected beam energy ends up in the tail of the energy spectrum of the background ions.

## Simulation and theory

The experimental observations described above clearly indicate that the fast ions are exciting a wave that couples to the plasma ions to create a tail in the energy distribution without any accompanying deleterious effects to bulk plasma confinement (there is no observable increase in magnetic flux or particle inventory decay rates). What is not clear from the measurement is whether this is a global or local phenomenon, and, if local, where in the plasma the mode is most active. For this, we turn to simulation.

We model the problem as an initial value problem in the PIC code EPOCH[21]. In the simulation, the wavevector is perpendicular to the magnetic field. The thermal plasma is Maxwellian without any drift. The hydrogen beam is a drifting Maxwellian with drift velocity corresponding to the injection energy in the experiment, 15 keV (see Methods for more details).

The dispersion relation from a PIC simulation is shown in Fig. 5a. When conditions approximating the mirror plasma are simulated (that is, when $\beta$, the ratio of the plasma pressure to the magnetic pressure is 10%), many harmonics of the ion cyclotron frequency emerge and the mode is identified as the Ion Bernstein

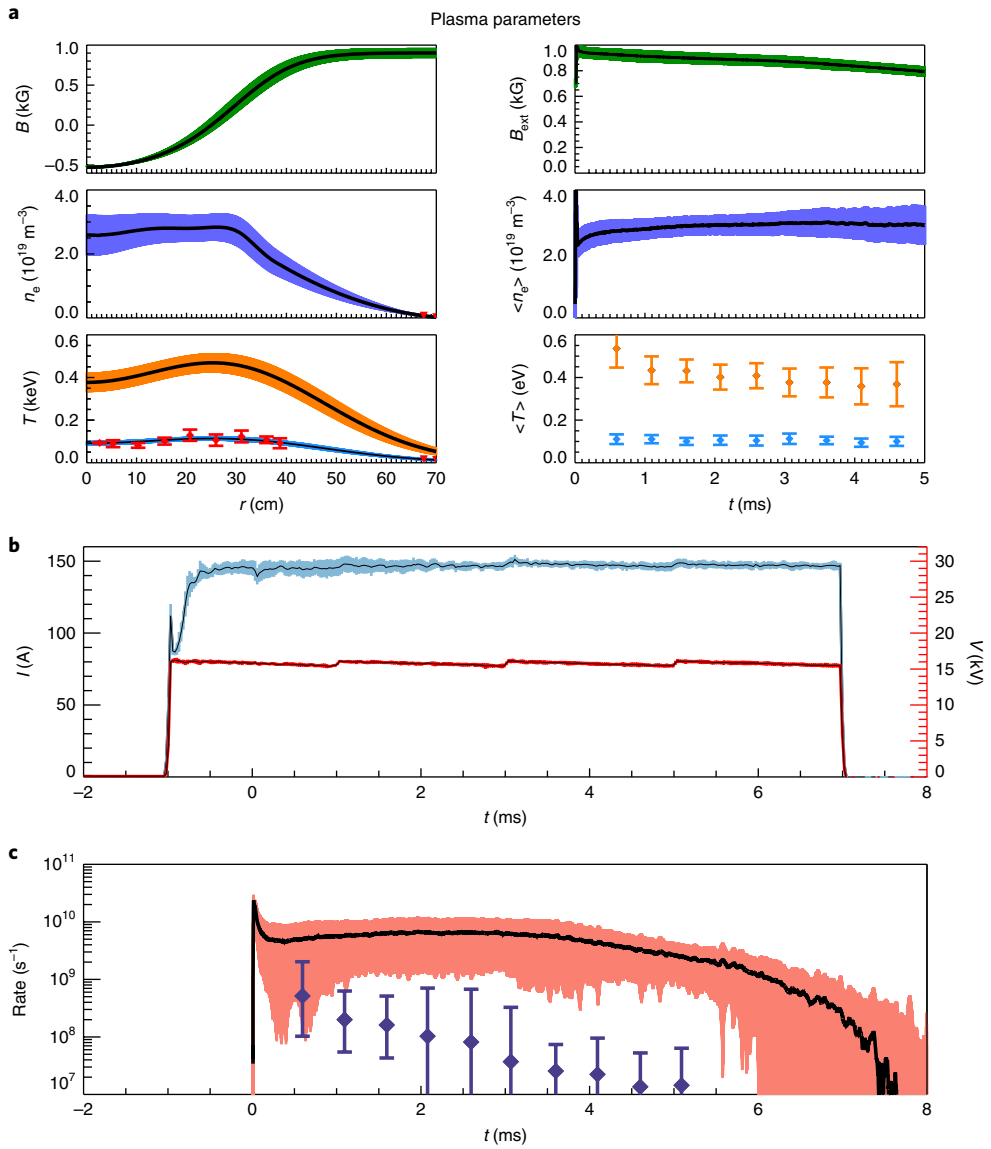


**Fig. 2 | Basic plasma and NBI parameters, and a comparison of the measured and calculated neutron emission rates. a**, Radial profiles (left column, taken at $t=1.5$ ms)) and time histories (right column) of plasma parameters averaged over 57 similar shots. Top row: rigid rotor magnetic field profile (note that the internal magnetic field is not measured) and external magnetic field as a function of time. Middle row: Abel-inverted electron density and the time history of the average density inside the FRC. Bottom row: electron temperature profile measured by Thomson scattering (red diamonds), by an edge Langmuir probe (red triangles) and the interpolated profile used in the fusion rate calculation (black line with blue error bars). The upper limit ion temperature profile is shown with orange error bars. The right panel shows the time history of the temperatures at the field null, with ions in orange and electrons in blue. **b**, NBI current (black line with cyan error bars, left axis) and voltage (red line, right axis), both averaged over the five beams. **c**, Measured neutron rate (black line with salmon error bars) and calculated thermonuclear fusion rate (purple diamonds). In all cases, error bars represent s.d. of the mean.

wave. This mode propagates nearly perpendicularly to the magnetic field at harmonics of the ion cyclotron frequency.

The ion velocity distribution output from the mirror plasma simulation is shown in Fig. 5b. As the simulation evolves, the modes grow and one can see a high-energy tail drawn out from the main ion energy distribution in a time much shorter than the beam slowing down time. This tail is small enough to have a negligible effect on the macroscopic distribution (that is, the temperature as determined by a Gaussian fit does not change, as illustrated by the solid lines), but large enough to have a significant impact on the fusion reactivity, due to the sensitive dependence of the fusion cross-section on particle energy. Figure 5c shows the fusion rate calculated by numerically summing over binary collisions. It can be seen that in 8 μs, less than 1/100th of a beam slowing down time, the fusion reaction rate is increased by a factor of 30 above thermonuclear.

Based on the high-energy tail and enhanced fusion observed in this simulation, we conclude that the beam-driven mode is probably more active in the mirror plasma than in the core. This localization may also explain why the fluctuations do not degrade confinement of the FRC core.

A simple criterion based on Wakefield theory[22] can be used to estimate the size of the wave electric field of the saturated ion Bernstein mode. In Wakefield theory, the mode amplitude saturates at the Tajima–Dawson field, $E=m_e c\omega_p/e$, where $m_e$ is the electron mass, $c$ is the speed of light, $\omega_p$ is the plasma frequency and $e$ is the electron charge. Simply put, the maximum velocity a

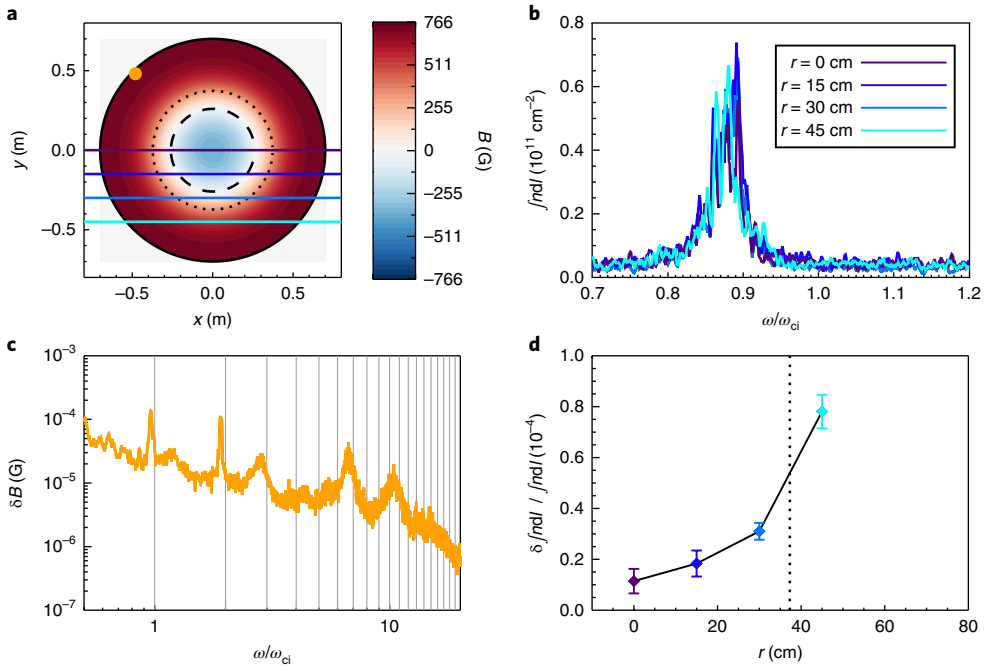


**Fig. 3 | Summary of measurements of fluctuations in the electron density and magnetic field associated with the beam-driven mode. a**, An ideal magnetic equilibrium shows the magnetic field strength (colour map), separatrix (dotted line) and field null (dashed line), as well as the measurement locations of the density (coloured horizontal lines) and magnetic field (orange dot). **b**, Density fluctuation spectra show a clear peak near the ion cyclotron frequency, $\omega_{ci}$, at all radii, even those outside the separtrix. **c**, Magnetic fluctuation spectrum, showing that multiple harmonics of $\omega_{ci}$ are excited. **d**, Size of the density fluctuations relative to the mean density peaks outside the separatrix. Error bars are propagated from the s.d. of the time-averaged line-integrated density and the 1$\sigma$ error estimate of a Gaussian fit to the frequency spectrum.

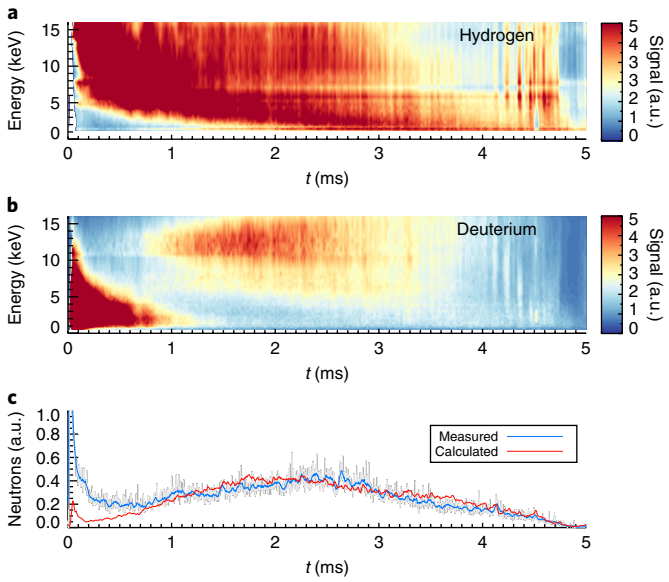


**Fig. 4 | Measurements of the energy spectra of charge exchange neutrals at the edge of the plasma reveal ion acceleration coincident with a rise in neutron emission. a**–**c**, Neutral hydrogen (beam species) energy spectrum (**a**), neutral deuterium (plasma species) energy spectrum (**b**) and measured (blue with grey error bars representing s.d. of the mean) and calculated (red) neutron flux (**c**). The calculated neutron flux is obtained from the measured deuterium energy spectrum.

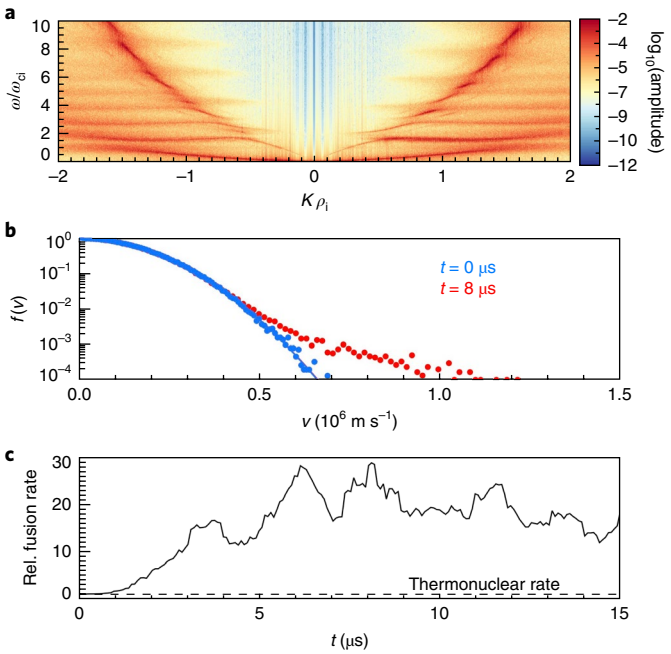


**Fig. 5 | Simulation of the beam-plasma system reveals the three features observed in experiment: fluctuations at harmonics of the ion cyclotron frequency, a high-energy tail on the main ion species and enhanced neutron production. a**, Dispersion relation from PIC simulation of $\beta = 0.1$ plasma showing the excitation of multiple ion Bernstein modes at harmonics of the ion cyclotron frequency. **b**, Plasma ion velocity distributions at $t = 0$ (blue) and $t = 8\,\mu s$ (red) in the simulation. The Gaussian fits for each time are plotted as solid lines and overlay each other. **c**, Corresponding neutron rate, normalized to the thermonuclear rate, as a function of time. The generated tail enhances the fusion rate by a factor of nearly 30.

particle can obtain from electric field acceleration in a wave period is the phase velocity. By making the substitutions $m_e \rightarrow M$, $c \rightarrow v_\phi$ and $\omega_p \rightarrow \omega_{ci}$ we obtain the ion Bernstein analogue, $E_{sat} = M v_\phi \omega_{ci}/e$, where $M$ is the deuteron mass, $v_\phi$ is the wave phase velocity and

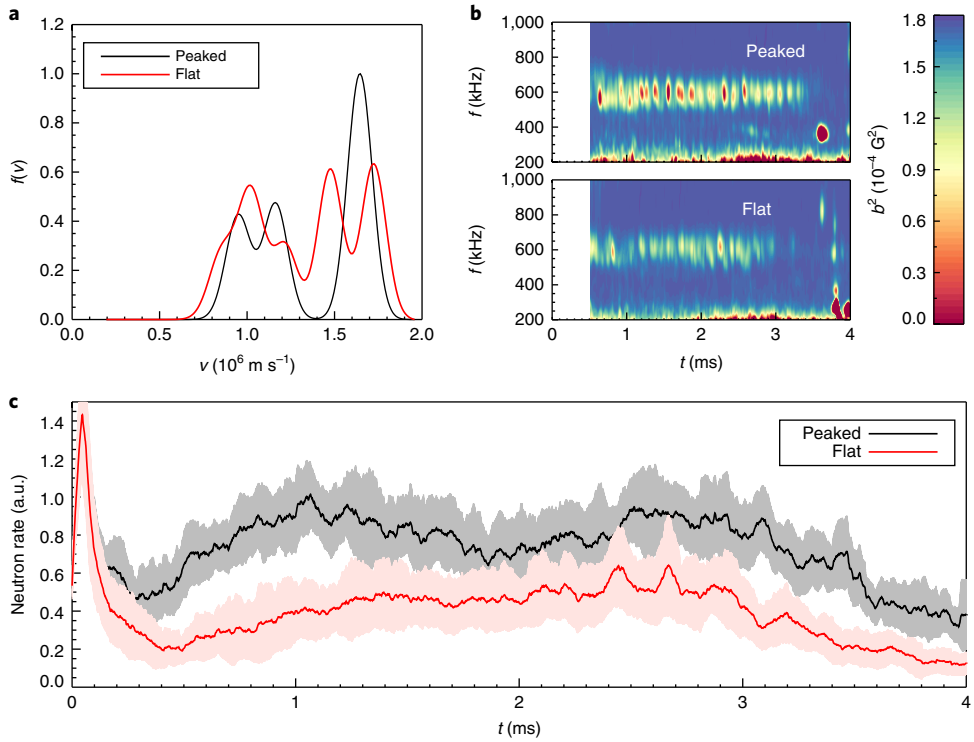


**Fig. 6 | Controlling mode activity by reducing velocity space gradients. a**, Calculations of the initial velocity distributions show the difference between the peaked (black curve) and flat (red curve) cases. **b**,**c**, The magnetic fluctuations (**b**) and neutron rates (**c**) are greatly reduced in discharges with reduced initial velocity space gradients. Error bars in **c** (shaded area) represent s.d. of the mean.

$\omega_{ci}$ is the ion cyclotron frequency. This simple estimate yields $E_{sat} = 3.6 \times 10^5\,\mathrm{V\,m^{-1}}$ for $v_\phi = 0.5 v_b$, close to the value found in simulation, $E_{sat} = 1.6 \times 10^5\,\mathrm{V\,m^{-1}}$.

## Experiment

A key prediction of the model is that free energy in the beam drives the wave fluctuations and the orders-of-magnitude fusion enhancement. To test this prediction an experiment was designed in which a source of free energy in the beam was varied, in this case $\partial f/\partial v$.

The neutral beam has three energy components due to the acceleration of $H_2$ and $H_3$ molecules in the beam line, in addition to the primary $H_0$ atomic species. The energy components are measured to be 85% full energy, 10% half energy and 5% third energy. The primary energy can be varied, and with five neutral beams it is possible to flatten the total fast ion velocity distribution by staggering the primary beam energy from beam to beam. We compared two cases, one in which all neutral beams have the same primary energy (14.4 kV) and one in which the beams are staggered (two at 11.5 kV and three at 16.0 kV). In each of the two cases the total injected current and power were the same (6.8 MW).

To assess the difference in free energy between the two cases, we define a parameter to quantify both the steepness and extent of the velocity space gradient as, $\alpha = \int \mathrm{d}v \partial f/\partial v$, where the integral is performed over regions of positive gradient. For the peaked case, $\alpha = 2.5$ and in the flat case, $\alpha = 1.8$, a reduction of 1.4×.

The results of the experiment are summarized in Fig. 6. Figure 6a presents the calculated initial velocity distributions for the two cases. It can be seen that in the 'peaked' case (black curve), larger positive gradients are present than in the 'flat' case (red curve). The magnetic fluctuation spectrograms are compared in Fig. 6b. The peaked case clearly has more activity in the ion cyclotron frequency band (in both cases, the fluctuations die out at around $t = 3$ ms). Finally, in Fig. 6c the measured neutron rates in each of the two cases are compared. The fusion enhancement is larger in the peaked case, by a factor of almost 2.

## Discussion

We can now summarize the key ingredients required for generating the beam-driven wave: tangential NBI, a large population of supra-Alfvénic fast ions with large orbits, and a positive velocity space gradient. Fokker–Planck modelling has shown that if the fast ion slowing down time is too fast, velocity space gradients are quickly smoothed out and there is no free energy source for the wave. This explains why the mode is not observed in cooler, denser plasmas.

The number of suprathermal ions accelerated by the mode is small compared to the plasma inventory, but it makes an outsized impact on fusion reactivity due to the extreme sensitivity of the cross-section in this energy range. In principle, this effect could be exploited to increase the energy output of a fusion reactor or the fluence of a neutron source.

There is, however, a more important possible fusion-relevant application of this mechanism: alpha channeling[23]. One of the issues facing burning plasma sustainment is the control of alpha particles, the high-energy products of the deuterium–tritium fusion reaction. The alphas are non-fusile, so they must be removed from the core to prevent ash accumulation and fuel dilution. However, to maintain high plasma temperature it is necessary that they first deposit their energy to the plasma. It may be possible to achieve both of these goals with 'phase space engineering', which uses a fast ion-driven wave to channel energy from fast alphas directly to the fusion fuel ions.

## Online content

Any methods, additional references, Nature Research reporting summaries, source data, statements of data availability and associated accession codes are available at https://doi.org/10.1038/s41567-018-0389-0.

Received: 21 February 2017; Accepted: 30 November 2018;
Published online: 14 January 2019

## References

1. Tuszewski, M. Reversed field configurations. *Nucl. Fusion* **28**, 2033–2092 (1988).
2. Rosenbluth, M. N., Krall, N. A. & Rostoker, N. Finite larmor radius stabilization of 'weakly' unstable confined plasmas. *Nucl. Fusion Suppl.* **1**, 143–150 (1962).
3. Binderbauer, M. W. et al. A high performance field-reversed configuration. *Phys. Plasmas* **22**, 056110 (2015).
4. Binderbauer, M. W. et al. Dynamic formation of a hot field reversed configuration with improved confinement by supersonic merging of two colliding high beta compact toroids. *Phys. Rev. Lett.* **105**, 045003 (2010).
5. Binderbauer, M. W. et al. Recent breakthroughs on C-2U: Norman's legacy. *AIP Conf. Proc.* **1721**, 030003 (2016).
6. Gota, H. et al. Achievement of field-reversed configuration plasma sustainment via 10 mW neutral-beam injection on the C-2U device. *Nucl. Fusion* **57**, 116021 (2017).
7. Guo, H. Y. et al. Achieving a long-lived high-beta plasma state by energetic beam injection. *Nat. Commun.* **6**, 6897 (2015).
8. Schmitz, L. et al. Suppressed ion-scale turbulence in a hot high plasma. *Nat. Commun.* **7**, 13860 (2016).
9. Heidbrink, W. W. Basic physics of Alfvén instabilities driven by energetic particles in toroidally confined plasmas. *Phys. Plasmas* **15**, 055501 (2008).
10. Belova, E. V. et al. Coupling of neutral-beam-driven compressional Alfvén eigenmodes to kinetic Alfvén waves in NSTX tokamak and energy channeling. *Phys. Rev. Lett.* **115**, 015001 (2015).
11. Anderson, J. K. et al. Fast ion confinement and stability in a neutral beam injected reversed field pinch. *Phys. Plasmas* **20**, 056102 (2013).
12. Gates, D. A., Gorelenkov, N. N. & White, R. B. Ion heating by fastparticle-induced Alfvén turbulence. *Phys. Rev. Lett.* **87**, 205003 (2001).
13. Berk, H., Horton, W., Rosenbluth, M. N. & Rutherford, P. H. Microinstability theory of two-energy-component toroidal systems. *Nucl. Fusion* **15**, 819–844 (1975).
14. Magee, R. M. et al. Absolute calibration of neutron detectors on the C-2U advanced beam-driven FRC. *Rev. Sci. Instrum.* **87**, 11D815 (2016).
15. Roche, T. et al. Enhanced magnetic field probe array for improved excluded flux calculations on the C-2U advanced beam-driven field-reversed configuration plasma experiment. *Rev. Sci. Instrum.* **87**, 11D409 (2016).
16. Beall, M., Deng, B. & Gota, H. Improved density profile measurements in the C-2U advanced beam-driven field-reversed configuration (FRC) plasmas. *Rev. Sci. Instrum.* **87**, 11E128 (2016).
17. Wesson, J. *Tokamaks* 3rd edn 246–253 (Clarendon Press, Oxford, 2004).
18. Deng, B. H. et al. High sensitivity far infrared laser diagnostics for the C-2U advanced beam-driven field-reversed configuration plasmas. *Rev. Sci. Instrum.* **87**, 11E125 (2016).
19. Clary, R. et al. A mass resolved, high resolution neutral particle analyzer for C-2U. *Rev. Sci. Instrum.* **87**, 11E703 (2016).
20. Matsuura, H. & Nakao, Y. Distortion of bulk-ion distribution function due to nuclear elastic scattering and its effect on T(d,n)$^4$He reaction rate coefficient in neutral-beam-injected deuterium-tritium plasmas. *Phys. Plasmas* **14**, 054504 (2007).
21. Arber, T. D. et al. Contemporary particle-in-cell approach to laser-plasma modelling. *Plasma Phys. Control Fusion* **57**, 113001 (2015).
22. Tajima, T. & Dawson, J. M. Laser electron accelerator. *Phys. Rev. Lett.* **43**, 267 (1979).
23. Fisch, N. J. The alpha channelling effect. *AIP Conf. Proc.* **2015**, 020001 (2015).

## Acknowledgements

The authors thank the investors for their support of TAE Technologies and the TAE and Budker teams for their contributions to this project. Special thanks go to E. Granstedt and E. Trask for help with the design of the experiment. This research used resources of the Oak Ridge Leadership Computing Facility, which is a DOE Office of Science User Facility supported under contract no. DE-AC05-00OR22725.

## Author contributions

R.M.M. contributed neutron measurements and neutron calculations, created all the figures and wrote the majority of the text. A.N. ran the PIC simulations, provided output data, and provided text for the 'Simulation and theory' section. R.C. provided NPA measurements. S.K. provided neutral beam injection. S.N. provided the analytical theory for benchmarking. T.R. and M.C.T. provided magnetic data. M.W.B. is the driving force behind the C-2U device and helped edited the text. T.T. provided theoretical interpretation of the experimental and simulation data and contributed significantly to the editing of the text.

## Competing interests

TAE Technologies, Inc. is a private corporation owned and financially supported by its shareholders. Some or all of the authors of this manuscript may have a financial interest in the company.

## Additional information

**Reprints and permissions information** is available at www.nature.com/reprints.

**Correspondence and requests for materials** should be addressed to R.M.M.

**Publisher's note:** Springer Nature remains neutral with regard to jurisdictional claims in published maps and institutional affiliations.

## Methods

We present four experimental measurements (neutron flux, neutral particle energy spectra, and density and magnetic fluctuations), two calculations (thermonuclear fusion rate and energetic tail fusion rate) and one computer simulation (EPOCH PIC code). The methods for each are described in the following sections. The plasma under study is a unique FRC plasma formed by the supersonic merger of two theta-pinches and sustained with NBI. The techniques for creating the plasma are described in ref. [4].

**Neutron measurements.** The 2.45 MeV neutrons are a product of the deuterium–deuterium fusion reaction. Their mean free path in stainless steel (SS316L) is 2.6 cm (ref. [24]), so the 1.3 cm confinement vessel is effectively transparent and the neutron detector can be conveniently located outside the vacuum boundary. The detector was mounted to the outside of the vacuum vessel near the north beam injection plane. The detection element was a 2 in. by 24 in. cylindrical plastic scintillator from Eljen Technology (EJ-200) coupled to a photomultiplier tube (PMT; model H6614-70 from Hamamatsu Corporation), designed for use in high magnetic fields. The PMT was operated with a bias voltage of 1.5–2.0 kV. The current signal output from the PMT was run through a 5 kΩ resistor to ground, and a unity gain operational amplifier (BUF634 from Texas Instruments) was used as a line driver to transmit the voltage signal to a D-TACQ analog-to-digital convertor with digitization rate of 1.5 MS s$^{-1}$.

The detector was absolutely calibrated using two independent, in situ methods. The first method involved firing each of six deuterium-fueled neutral beams individually into a high-density ($10^{14}$ cm$^3$) deuterium gas target. The measured signal on the detector was then compared to the output of a Monte Carlo code used to simulate fast ions in the plasma. In this application, the magnetic field and plasma density in the simulation were set to zero so the code calculated the fusion rate due to the beam in the neutral gas. The second method was to insert a probe-mounted AmBe source into the vented vacuum vessel and measure the signal at 50 different locations. The two methods agreed well, giving a calibration factor of $2.4 \pm 1.4 \times 10^7$ n s$^{-1}$ V$^{-1}$ and $2.6 \pm 0.4 \times 10^7$ n s$^{-1}$ V$^{-1}$, respectively. The calibration procedure is detailed in ref. [14].

The time history of an average of the neutron rate over 57 shots is plotted in the black trace in Fig. 2c. A set of seven shots are plotted in the blue trace in Fig. 4c. The final data from the neutron detector are presented as two traces, red and black, from the staggered beam energy experiments plotted in Fig. 6c, as averages of three and four shots, respectively.

**Neutral particle measurements.** Neutral spectral flux measurements rely on energetic ions in the plasma that charge-exchange with neutral particles ($H^0$) primarily concentrated at the outer boundary of the FRC plasma. These energetic, charge-exchanged particles are immune to the confining magnetic field of the experiment and promptly escape the system, a portion of which enter the NPA diagnostic system. The NPA view intersects the confinement chamber wall ~65 cm from the confinement chamber midplane, has an impact parameter of 49 cm, and is oriented relative to the machine axis to match the expected energetic ion trajectories. The NPA view does not intersect any NBI ports.

On entering the diagnostic, charge-exchanged particles are re-ionized in a He-filled gas chamber (~3 mtorr), permitting analysis via electric and magnetic fields established inside the device. The particles are dispersed according to energy by a user-controlled magnetic field perpendicular to the particle trajectory. A user-controlled electric field parallel to the magnetic field disperses the particles according to mass. In this manner energy distributions of charge-exchanged deuterons and protons can be distinguished simultaneously as a function of time for the duration of the experiment.

Particles are registered on a dual-stage micro-channel plate (MCP) system, biased at −2 kV (~1 kV bias per stage). The MCP detection system is operated in current mode, producing an output current proportional to particle flux with ~$10^7$ gain. The MCP signal is amplified and digitized (1 MΩ gain, <10 μs response time) by an integrated device developed at TAE[19].

Figure 4a,b shows the energy distributions for neutral hydrogen and deuterium, respectively, averaged over four shots. The calculated neutron rate shown in Fig. 4c is computed using the deuterium distribution data shown in Fig. 4b, as described in 'Calculation of energetic ion-enhanced fusion rate'.

**Magnetics measurements.** Charged particle motion generates magnetic fields. High-frequency fluctuations in the magnetic field are detectable at the very edge of the plasma on the wall of the confinement vessel, but are stronger closer to the core plasma. We measured the edge magnetic fluctuations with wall-mounted coils and the interior fluctuations with an insertable magnetic probe. The wall-mounted coils are composed of three coils of wire for each orthogonal direction of magnetic field arranged in an azimuthal array of eight coils at $z = 25$ cm (ref. [25]). The $\theta$ direction is chosen for the fluctuation study because the equilibrium $B_\theta$ is small, allowing small fluctuations to be resolved. Figure 6b shows the average wavelet spectrogram for two sets of shots (the spectrograms are averaged over coil number and shot number). The IDL routine WV_CWT with a 12th-order Morlet mother wavelet and dscale = 0.02, nscale = 500 and $f_{max} = 2$ MHz produces each spectrogram. The probe is composed of high-vacuum-compatible ceramic chip inductors from Coilcraft CPS mounted on ceramic (Rogers 4003) printed circuit boards (PCBs) which produce a voltage in the presence of changing magnetic fields. Such a PCB is designed with two inductors (AE450RAA683GSZ and AE450RAA333GSZ) oriented so as to detect $dB_\theta/dt$ and $dB_z/dt$, respectively[25]. The inductors are standard 1812 surface mount chip size. The PCB is 3 in. long. The circuit board is mounted to an in-vacuum linear translation stage from Thermionics Inc. (FLMH-275-50-24) with a stroke length of 24 in. This system allows the probe to be positioned anywhere from flush with the vessel wall ($r = 70$ cm) to a radius inside the scrape off layer of the plasma ($r = 45$ cm). The PCB assembly is protected from the plasma with a quartz tube. The probe signals are carried on screened, shielded twisted-pair cable terminated in 50 Ω and digitized by National Instruments digitizers (PXIe-5105) at a rate of 60 MS s$^{-1}$. Figure 3c shows the discrete fast Fourier transform (performed with IDL routine FFT) of the partial time history ($t = 0.5$–$1.5$ ms) of a single shot with the probe inserted 3 cm from the vessel wall.

**Density measurements.** The density measurements shown in Fig. 3b,d are obtained from the FIR laser interferometer[18]. The system employs a $CO_2$ pump laser and two formic acid vapour FIR lasers (a probe beam and a reference beam) with wavelength $\lambda = 433$ μm. The probe beam is split into four chords with impact parameters 0, 15, 30 and 45 cm. An additional two-colour $CO_2$/HeNe interferometer is used to compensate for vibration.

The spectra plotted in Fig. 3 are obtained by performing a discrete fast Fourier transform on the detrended time histories of shot 43,393 from $t = 1$ to $t = 3$ ms using the FFT function in IDL. The peak in the spectra are fit with a four-term Gaussian (that is, Gaussian plus d.c. offset) using the GAUSSFIT IDL function. The profile (Fig. 3d) is then obtained by dividing the amplitude of the Gaussian by the mean value of the line-integrated density over the same time window.

**Calculation of thermonuclear fusion rate.** The thermonuclear fusion rate, plotted as the purple diamonds in Fig. 2c, is calculated using $R = \frac{1}{2} 2\pi L_{FRC} \int n_i(r)^2 <\sigma v> (T_i(r)) r\,dr$, where $n_i$ is the ion density, which we obtain by assuming that $n_i \sim n_e$ and measure $n_e$ with interferometry[18], using the central chord and dividing by the separatrix radius to give the central line-averaged density. The fusion reaction rate, $<\sigma v>$ is a known function[26] of ion temperature, which we obtain from $T_i = T_{tot} - T_e$, where $T_{tot}$ is the total temperature derived from radial pressure balance (that is, FRC volume averaged pressure) and $T_e$ is measured with Thomson scattering[27]. Only two time points of electron temperature data are obtained per plasma discharge on C-2U, so the time history is built up by pulsing the laser at different times in each of 57 similar discharges. Finally, $L_{FRC}$ is the length of the FRC obtained from magnetic measurements[25].

**Calculation of energetic ion-enhanced fusion rate.** The energetic ion-enhanced fusion rate (red curve in Fig. 4c) is calculated using $R \sim \int dE f(E) \sigma_{DD}(E) v$ where $f(E)$ is the NPA energy spectrum, $\sigma_{DD}$ is the fusion cross-section[26] and $v$ is the energetic ion velocity (plasma temperature is ignored here). Because the NPA is not absolutely calibrated, magnitudes cannot be compared. The curve is scaled to best match the measured flux.

**PIC simulation.** EPOCH is a fully electromagnetic three-dimensional and three-velocity (3D3V) PIC code capable of running on 100,000 cores and able to self-consistently resolve the effects of electromagnetic fields on the electron and ion orbits and then feedback the orbits' effects on the fields. As with many other PIC codes it may be decomposed into three components: particle pusher, particle/current deposition and advancement of Maxwell's equations.

Particle push uses the Boris algorithm[28]. Particle/current deposition is carried out via the Esirkepov method[29], and the standard finite-difference time-domain (FDTD) technique is used to advance Maxwell's equations numerically. $E$ and $B$ fields are specified on the staggered Yee mesh[30]. EPOCH uses high-order B-spline for the shape functions for particles. Each simulation particle is a macro-particle containing millions of physical particles. A fast Fourier transform of the time and space fluctuations of the fields on the grid is taken at the end of the simulation to analyse wave activity. This is the contour plot shown in Fig. 5a.

For a given set of physical parameters, the simulation approach of EPOCH is compared with analytical and semi-analytical techniques. In the analytical approach, simple $\omega(k)$ relations (usually made in the approximation of a cold plasma) are overlaid with the EPOCH results to verify general physical phenomena. In the semi-analytical approach, a more complicated dispersion relation, such as is given by the rank-three, kinetic dielectric tensor, is solved over a given domain of $k$ and $\omega + iy$ using the winding number method.

In particular, for each of an array of $k$ values, the dispersion relation is probed for solutions over a grid of sampling points in the complex plane for $\omega$ and $y$. One rectangular cell of four points is considered at a time. Using many intermediate sample points, as is necessary to provide smooth mapping, the dispersion relation is mapped over the closed contour formed by the four edges of the cell. If the winding number around the origin of the resulting mapped contour is non-zero, the original rectangular cell of sample points contains at least one solution. Once the full sample grid has been probed for all $k$ values, the cells that contain solutions are themselves examined in a similar manner to refine the solutions.

## Data availability

The data that support the plots within this paper and other findings of this study are available from the corresponding author upon reasonable request.

## References


24. Goorley, T. Initial MCNP6 release overview. *Nucl. Technol.* **180**, 298–315 (2012).
25. Thompson, M. C. et al. Magnetic diagnostic suite of the C-2 field-reversed configuration experiment confinement vessel. *Rev. Sci. Instrum.* **83**, 10D709 (2012).
26. Bosch, H.-S. & Hale, G. M. Improved formulas for fusion cross-sections and thermal reactivities. *Nucl. Fusion* **32**, 611–631 (1992).
27. Zhai, K. et al. The upgrade of the Thomson scattering system for measurement on the C-2/C-2U devices. *Rev. Sci. Instrum.* **87**, 11D602 (2016).
28. Boris, J. P. Relativistic plasma simulation-optimization of a hybrid code. in *Proc. 4th Conference on Numerical Simulation of Plasmas* 3–67 (1970).
29. Esirkepov, T. Zh. Exact charge conservation scheme for particle-in-cell simulation with an arbitrary form-factor.*Comput. Phys. Commun.* **135**, 144–153 (2001).
30. Yee, K. S. Numerical solution of initial boundary value problems involving Maxwell's equations in isotropic media. *IEEE Trans. Antennas Propag.* **14**, 302–307 (1966).